Int. J. Heat Mass Transfer. Vol. 22, pp. 1069–1081
Pergamon Press Ltd. 1979. Printed in Great Britain

HEAT AND MASS TRANSFER IN POROUS MEDIA SUBJECT TO FIRES

M. S. SAHOTA
Idaho National Engineering Laboratory, Idaho Falls, ID 83401, U.S.A.

and

P. J. PAGNI
Department of Mechanical Engineering, University of California, Berkeley, CA 94720, U.S.A.

(*Received* 10 *August* 1978 *and in revised form* 26 *December* 1978)

Abstract—The transient solution of two-phase, two-component flow in one-dimensional or axi-symmetric porous concrete structures exposed to time-dependent nonlinear mixed boundary conditions has been obtained. The basic mechanisms considered in the theory are: heat conduction through all the components, the molecular diffusion of the gaseous components, and the pressure driven convective flow governed by Darcy's law. The governing heat and mass transfer equations are solved numerically by an implicit finite difference scheme. A simplified technique for calculating the temperature field is developed and the results compare favorably with the complete analysis. The temperature fields for dry and wet cases do not differ significantly for normal amounts of moisture content in concrete. General results are given for two limiting fire histories, the American Society for Testing and Materials E-119 time–temperature curve and a short-duration, high-intensity time–temperature curve. Comparisons are made between experimental and theoretical temperature fields in a wet, porous, alumina powder system. Good agreement is obtained. Applications to structural fires and a variety of other heat and mass transfer problems are discussed.

NOMENCLATURE

a, b, c, d, coefficients in equation (20);
A, B, C, constants in Clausius–Clapeyron equation;
Bi, hL/k, Biot number;
c_p, specific heat at constant pressure; $[\mathrm{J\,kg^{-1}\,K^{-1}}]$;
$\bar{c}_p$, c_p/c_{p0}, dimensionless specific heat at constant pressure;
C_r, $\rho_m c_{pm}/(\rho c_p)$, heat capacity ratio;
D, diffusion coefficients for Fick's law for air–vapor mixture $[\mathrm{m^2\,s^{-1}}]$;
$\bar{D}$, D/D_0, dimensionless diffusion coefficient;
f, effective shape factor for radiation;
F, $\theta_f + \theta_f^4 St/Bi$, fire temperature group;
h, convective heat transfer coefficient $[\mathrm{J\,s^{-1}\,m^{-2}\,K^{-1}}]$;
h_D, mass transfer coefficient $[\mathrm{kg\,s^{-1}\,m^{-2}}]$;
h_{fg}, heat of evaporation of water $[\mathrm{J\,kg^{-1}}]$;
$\bar{h}_{fg}$, $h_{fg}/(c_{p0} T_{f,0})$, dimensionless heat of evaporation of water;
k, thermal conductivity $[\mathrm{J\,s^{-1}\,m^{-1}\,K^{-1}}]$;
$\bar{k}$, k/k_0, dimensionless thermal conductivity;
k_D, Darcy's coefficient $[\mathrm{m^3\,s\,kg^{-1}}]$;
$\bar{k}_D$, $k_D p_\infty/\alpha_0$, dimensionless Darcy's coefficient;
L, length for plane geometry and outer radius for cylindrical geometry [m];
Le, D_0/α_0, modified Lewis number;
p, pressure $[\mathrm{N\,m^{-2}}]$;
$\bar{p}$, p/p_∞, dimensionless pressure;
r, 1 for geometry, and x or $\bar{x}$ for cylindrical geometry;
R, gas constant per unit mass $[\mathrm{J\,kg^{-1}\,K^{-1}}]$;
Sh, $h_D L/(\rho_m D)$, Sherwood number;
St, $\sigma f L T_{f,0}^3/k$, modified Stefan number;
t, time [s];
$\bar{t}$, $t\alpha_0/L^2$, dimensionless time;
T, absolute temperature [K];
u, velocity $[\mathrm{m\,s^{-1}}]$;
$\bar{u}$, uL/α_0, dimensionless velocity;
w_i, ρ_i/ρ_m, mass fraction of specie i with respect to the density of air–vapor mixture;
$\bar{w}_i$, $w_i/w_{a\infty,0}$, ratio of the mass fraction of specie i to the initial ambient mass fraction of air;
x, distance [m];
$\bar{x}$, x/L, dimensionless distance.

Greek symbols

α, $k/(\rho c_p)$, thermal diffusivity $[\mathrm{m^2\,s^{-1}}]$;
$\bar{\alpha}$, α/α_0, dimensionless thermal diffusivity;
Γ_i, production rate of specie i per unit total volume $[\mathrm{kg^{-3}\,s^{-1}}]$;
$\bar{\Gamma}_i$, $\Gamma_i L^2/(\rho_0 \alpha_0)$, dimensionless rate of production of special i;
ε, void volume/total volume, porosity;

θ, $T/T_{f,0}$, dimensionless temperature;
ρ, mass per unit total volume, density [kg m^{-3}];
$\bar{\rho}$, ρ/ρ_0, dimensionless density;
ρ_i^*, mass of specie i per unit volume of specie i [kg m^{-3}];
σ, Stefan–Boltzmann constant [J s^{-1} m^{-2} K^{-4}].

Subscripts

a, air;
f, fire;
i, specie i;
l, liquid;
m, air–vapor mixture,
s, solid;
sat, saturation point for vapor;
v, vapor;
0, initial condition or datum;
∞, ambient.

INTRODUCTION

AN IMPORTANT problem in fire safety is determining the structural integrity of a building after a severe fire. Not all pertinent damage is visible, so it is necessary to predict the internal stresses which result from any given fire. The first step is to predict the thermal behaviour of the structure when subjected to a known fire. This thermal response then determines the internal stresses and therefore the structural safety.

The problem is complicated by the presence of moisture in concrete. The water inside the structure evaporates due to heating which in turn generates high pressures and strong concentration gradients. High pressure causes the gases (air and water vapour) to flow toward the surface. In addition, ambient air diffuses into the concrete structure to balance the concentration gradients developed during evaporation. Mass diffusion of water vapour also enhances the evaporation rates. The fields are described by the overall energy equation, a continuity equation for each component, Darcy's law for each phase, an equation of state for each gaseous component, and the transport property relations.

The study thus carried out has diverse industrial applications. Multiphase flow is of special interest to the petroleum industry due to its applicability to secondary petroleum recovery. Drying processes and transport of pyrolysed combustibles influence the burning of most natural, some synthetic polymers. Heat and mass transfer plays an important role in the stress calculations for the storage of radioactive waste in concrete enclosures. The flow of cavity gas following an underground nuclear explosion also falls in the same category. In general, the present analysis is applicable to any heat and mass transfer problem with phase change in a porous medium. With some modifications, the solution technique can be extended to heat transfer problems with internal chemical reactions.

The problem considered here is a concrete structure surrounded by a known fire with an external bounding surface as shown in Figs. 1a and b. The analysis is limited to one-dimensional or axisymmetric geometry due to the complexity of the problem. The simultaneous solution of the unsteady differential equations for porous media is required. This solution then serves as an input to the structural analysis. Since most structural effects occur after flashover, only this time period will be considered. As in the standard test methods [1, 2], the fire is described by a specified gas phase temperature history. The interaction between the fire and the structural element is described by a view factor, total emissivities of the fire, the element surface, the surrounding compartment surfaces, and a convective heat transfer coefficient. Sahota and Pagni [3] obtained a quasi-analytic solution of a two-dimensional conduction problem with time-dependent, nonlinear, mixed boundary conditions ignoring property variations and moisture transfer. Whether these effects dominate depends on the exact application. Bresler and co-workers [4–6] have approached the conduction problem, along with the internal stress problem, using the finite element method. Comparisons have been reported [3] with their numerical solutions and experimental data.

Most of the previous work for heat transfer in porous media is for single phase, either liquid or gas, flowing through the medium [7–13]. Luikov defined a system of coupled differential equations on the basis of thermodynamics of irreversible processes [14] and presented a set of solutions for several geometries and boundary conditions [15]. The validity of linear flux–force equations based on nonequilibrium thermodynamics in a closed system at steady state conditions, was investigated experimentally [16]. Chase *et al.* [17] solved a linear system of differential equations by making many simplifying assumptions for the case of regenerator type mass exchangers. Kumar [18] extended the variational formulation technique based on local potential to simplified nonlinear heat and mass transfer equations in a porous medium. Gupta [19], following Kumar, applied local potential and integral techniques by defining a moving evaporation front which divided the system into dry and wet regions. Murty *et al.* [20] solved the mass diffusion equation in a partially liquid filled porous matrix by Laplace transforms and contour integration. Kozdoba and Chumakov [21] obtained heat and mass transfer equations with an allowance for the difference between the coolant (air–vapor mixture) and the skelton (porous medium) temperatures for transpiration cooling. Solution techniques based on finite integral transforms [22] and the finite element method [23] have been obtained. Some experimental results pertaining to porous media such as, cotton [24], porous bronze [25], and the materials commonly used as protective coverings for steel in building construction such as, clay, concrete, gypsum, lime mortar, can be found in [26].

Most of the literature cited above does not take into account the pressure build up inside the porous medium due to evaporation and subsequent movement of the fluids. Rubin and Schweitzer [27] considered the flow of liquid from a reservoir at high pressure entering a porous medium which is heated from the other side causing evaporation of the liquid within the medium. But they ignored mass diffusion. Morrison [28] made an elaborate analysis applied to the cavity formed by underground nuclear explosions. Mass diffusion and heat conduction through the porous medium were neglected. Harmathy [29] reported heat and mass transfer caluclations at low temperatures for fire clay bricks and compared the results with experiments. Min and Emmons [30] presented an elegant but simple analysis presuppoposing a dry–wet interface, and compared the results with their experimental data on packed aluminum oxide powder. Saito and Seki [31] analyzed a one-dimensional moist porous material problem neglecting mass diffusion, postulating a dry–wet interface, and neglecting the volume occupied by the liquid.

In the present analysis, all the terms are initially included in the applicable differential equations. No dry–wet interface is postulated; however, the results obtained predict such an interface. The advantages of this are: (1) The problem of locating the dry–wet interface is eliminated, which is particularly useful in multi-dimensional systems; (2) no boundary conditions at the interface are required; and (3) the analysis is applicable to both kinds of problems, with and without inside discontinuities.

All the previous work known to the authors ignored the condensation of the vapor in the dry region. This condensation is possible if the temperature in the wet region exceeds the temperature in the dry region, as could be the case during the temperature fall portion of the fire time–temperature curve. The present analysis takes into account this phenomenon; however, it is not observed to be of critical significance.

Finally, an attempt has been made to simplify the governing equations by nondimensionalizing the system and comparing the relative magnitude of each term. A simple technique for caluclating the temperature field is then developed and found to accurately describe systems of practical import. When the pressure field calculation is not required, which is often the case, this simple technique is especially convenient.

THEORETICAL FORMULATION

Assumptions

The following assumptions are made for the theoretical model:

1. Local thermodynamic equilibrium exists. According to Morrison [28] the response time for local heat transfer between the fluid and the solid is several orders of magnitude smaller than the times of interest. Therefore the temperatures of the fluid and solid are the same at each point and the assumption of local thermodynamic equilibrium is valid. This makes a heat transfer model between fluid and solid unnecessary and provides an unambiguous definition of the temperature at a point.

2. Liquid–vapor equilibrium exists in the presence of free water, which makes the partial pressure of the vapor equal to the saturation pressure. A more accurate expression for the partial pressure can be used if the adsorption characteristics of the medium are known. This assumption is not a necessary feature of the theory and is made only because it is observed to be the case.

3. Movement of the liquid is neglected. This also is not an inherent feature of the theory and the liquid-movement can easily be incorporated given a Darcy's coefficient for the liquid. But the value of Darcy's coefficient for the movement of the liquid is so small compared to that of the gases, that the liquid movement is negligible. This is further substantiated by Harmathy [29] and Min and Emmons [30] who claim that the liquid, particularly at low moisture content, is present in the pendular state, that is, the liquid in different pores is not interconnected.

4. Evaporation of chemically and physically bound water is neglected. This assumption is again not a necessary feature of the theory. It is made in the absence of the detailed information on bound water kinetics.

5. Darcy's law with variable coefficient holds for gases. Usually, this law holds for steady flows under isothermal conditions. Schweitzer [32] modified it for nonisothermal conditions and noted his result simplified to the ordinary Darcy's law with variable coefficient if the viscosity was not a strong function

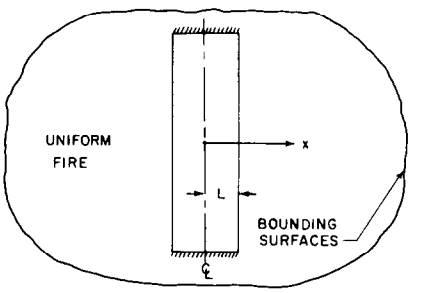

(a) PLANE GEOMETRY

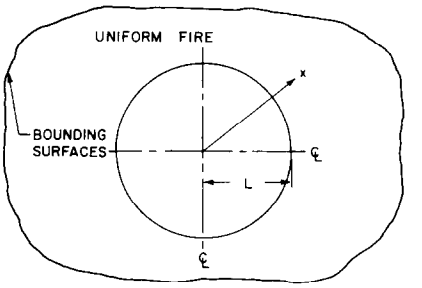

(b) AXI–SYMMETRIC GEOMETRY

FIG. 1. Alternative system geometries.

of temeperature. Rubin and Schweitzer [27] also modified Darcy's law for transient problems. Again they found the additional term to be negligible for all practical purposes due to small values of the Reynolds number encountered in porous media.

6. Air and water vapor are treated as ideal gases. All systems of interest are far from the critical point.

Analysis

The system considered is shown schematically in Figs 1a, b. The spatial uniformity of the fire introduces symmetry at the center of the structural element with zero flux conditions at this interior boundary. The results presented here use these conditions; however, the analysis can be easily modified for asymmetric problems.

The following governing equations and boundary conditions describe the complete system [33]. The final energy equation, after incorporating some simplifications involving mass conservation, is

$$\frac{\partial T}{\partial t} = \alpha \frac{\partial^2 T}{\partial x^2} + \left\{ \frac{1}{\rho c_p r} \frac{\partial}{\partial x}(rk) - \frac{\rho_m c_{pm}}{\rho c_p}\left[u_m + \frac{D(c_{pv} - c_{pa})}{c_{pm}} \frac{\partial w_a}{\partial x} \right] \right\} \frac{\partial T}{\partial x} - \frac{1}{\rho c_p}\left[h_{fg}\Gamma_m - \frac{\partial}{\partial t}(\rho_m R_m T) \right], \tag{1}$$

where k, ρ, c_p, and α are the overall values. The initial and boundary conditions are

$$T(x,0) = T_0(x), \tag{2}$$

$$\frac{\partial T}{\partial x}(0,t) = 0, \tag{3}$$

$$-k\frac{\partial T}{\partial x}(L,t) = h[T(L,t) - T_f(t)] + f\sigma[T^4(L,t) - T_f^4(t)]. \tag{4}$$

The species equation for air is given below. The one for vapor is omitted as only one species equation is needed if the overall air-vapor continuity is included.

$$\frac{\partial w_a}{\partial t} = D\frac{\partial^2 w_a}{\partial x^2} + \left[\frac{1}{\rho_m r}\frac{\partial}{\partial x}(r\rho_m D) - u_m \right] \times \frac{\partial w_a}{\partial x} - \frac{w_a \Gamma_m}{\rho_m}. \tag{5}$$

The initial and boundary conditions are

$$w_a(x,0) = w_{a,0}(x), \tag{6}$$

$$\frac{\partial w_a}{\partial x}(0,t) = 0, \tag{7}$$

$$-\rho_m D\frac{\partial w_a}{\partial x}(L,t) = h_D[w_a(L,t) - w_{a\infty}(t)] \tag{8a}$$

for dry surface, and

$$w_a(L,t) = \frac{1 - \frac{p_v}{p}(L,t)}{1 - \frac{R_v - R_a}{R_v} \times \frac{p_v}{p}(L,t)} \tag{8b}$$

for wet surface.

Equation (8b) has been obtained from the equations of state for vapor and air. When the surface is wet, the partial pressure of the vapor at the surface is equal to the saturation pressure. Thus $w_a(L,t)$ is explicitly known in that case. The velocity of the air–vapor mixture is given by

$$u_m = -k_D \frac{\partial p}{\partial x}, \tag{9}$$

with the boundary condition

$$p(L,t) = p_\infty. \tag{10}$$

The conservation of gas phase mass gives

$$\frac{\partial \rho_m}{\partial t} + \frac{1}{r}\frac{\partial}{\partial x}(r\rho_m u_m) = \Gamma_m, \tag{11}$$

with the boundary condition

$$u_m(0,t) = 0. \tag{12}$$

The continuity equation for the liquid is

$$\frac{\partial \rho_l}{\partial t} = \Gamma_l = -\Gamma_m, \tag{13}$$

with only the initial condition required,

$$\rho_l(x,0) = \rho_{l,0}(x). \tag{14}$$

Equations of state for the vapor and the air–vapor mixture are

$$p_v\left(\varepsilon - \frac{\rho_l}{\rho_l^*}\right) = (1-\omega_a)\rho_m R_v T \tag{15}$$

$$p\left(\varepsilon - \frac{\rho_l}{\rho_l^*}\right) = \rho_m R_m T. \tag{16}$$

Since liquid and vapor are assumed in equilibrium,

$$p_v = p_{\text{sat}}(T), \tag{17}$$

in the presence of liquid water. An analytic expression for p_{sat} is obtained by Sahota [33]. The result is

$$p_{\text{sat}}(T) = C T^{-B/R_v} \exp\left(\frac{-A}{R_v T}\right), \tag{18}$$

where $A = 3.18 \times 10^6\ \text{J kg}^{-1}$, $B = 2470\ \text{J kg}^{-1}\ \text{K}^{-1}$ and $C = 6.05 \times 10^{26}\ \text{N m}^{-2}$. This set of equations describes the heat and mass transfer problem in a porous medium. In summary, the equations to be solved are: energy, species equation for air, Darcy's law, mixture gas continuity, liquid continuity, two equations of state, and Clausius–Clapeyron equation (phase equilibrium). The unknowns are: temperature, air mass fraction, pressure, mixture mass average velocity, liquid density, mixture production rate, mixture density, and vapor partial pressure.

These eight governing equations with eight unknowns define the system completely. It is computationally convenient to recast these equations in terms of the pressure and to explicitly eliminate the evaporation term which does not have a simple Arrhenius type expression but rather is obtained

implicitly from the liquid–vapor equilibrium assumption. Differentiating equation of state (16) with respect to t and simplifying by making use of equation (13); substituting for $\partial\rho_m/\partial t$ from the resulting equation, u_m from equation (9), and $\partial\rho_l/\partial t$ from equation (13) into equation (11), one obtains,

$$\frac{\partial p}{\partial t} = pk_D\frac{\partial^2 p}{\partial x^2} + \frac{p}{\rho_m r}\frac{\partial}{\partial x}(r\rho_m k_D)\frac{\partial p}{\partial x} + \frac{\Gamma_m p}{\rho_m}\left(1-\frac{p}{\rho_l^* R_m T}\right) + \frac{p}{R_m T}\frac{\partial}{\partial t}(R_m T). \tag{19}$$

The above equation applies irrespective of whether the region is dry or wet. However, if the region is wet, Γ_m in equation (19) is not explicitly known. Thus it is useful to eliminate Γ_m from equation (19), and obtain an equation applicable in the presence of liquid. The result is

$$d\frac{\partial p}{\partial t} = a\frac{\partial^2 p}{\partial x^2} + b\frac{\partial p}{\partial x} - c, \tag{20}$$

where

$$a = D + pk_D\left[\frac{w_a R_a}{w_v R_m\left(1-\frac{p}{\rho_l^* R_m T}\right)} + \frac{p_v'}{p_v}\frac{\rho_m}{\rho c_p}\frac{\left(h_{fg}-\frac{p}{\rho_l^*}\right)}{\left(1-\frac{p}{\rho_l^* R_m T}\right)}\right], \tag{21}$$

$$b = \frac{p}{\rho_m r}\frac{\partial}{\partial x}(r\rho_m k_D)\left[\frac{w_a R_a}{w_v R_m}\left(1-\frac{p}{\rho_l^* R_m T}\right)^{-1} + \frac{p_v'}{p_v}\frac{\rho_m}{\rho c_p}\frac{\left(h_{fg}-\frac{p}{\rho_l^*}\right)}{\left(1-\frac{p}{\rho_l^* R_m T}\right)}\right] + 2D\left[\left(2\frac{R_m}{R_a}-1\right)\frac{1}{p_v}\frac{\partial p_v}{\partial x} + \frac{R_m}{R_a}\frac{u_m}{pk_D}\right] + \frac{1}{\rho_m r}\frac{\partial}{\partial x}(r\rho_m D) - u_m - pk_D\frac{1}{p_v}\frac{\partial p_v}{\partial x}, \tag{22}$$

$$c = p\left\{\frac{D}{p_v}\frac{\partial^2 p_v}{\partial x^2} - \alpha\frac{p_v'}{p_v}\frac{\partial^2 T}{\partial x^2} + \frac{1}{\rho_m r}\frac{\partial}{\partial x}(r\rho_m D)\frac{1}{p_v}\frac{\partial p_v}{\partial x} - \frac{p_v'}{p_v}\left[\frac{1}{\rho c_p r}\frac{\partial}{\partial x}(rk) - \frac{\rho_m c_{pm}}{\rho c_p}\left(u_m + D\frac{c_{pv}-c_{pa}}{c_{pm}}\frac{\partial w_a}{\partial x}\right)\right]\frac{\partial T}{\partial x} + 2D\left(\frac{R_m}{R_a}-1\right)\left(\frac{1}{p_v}\frac{\partial p_v}{\partial x}\right)^2 - \left[\frac{w_a R_a}{w_v R_m\left(1-\frac{p}{\rho_l^* R_m T}\right)} + \frac{p_v'}{p_v}\frac{\rho_m}{\rho c_p}\frac{\left(h_{fg}-\frac{p}{\rho_l^*}\right)}{\left(1-\frac{p}{\rho_l^* R_m T}\right)}\right]\times\left[\frac{1}{T} + \frac{w_v(R_v-R_a)}{R_a}\frac{p_v'}{p_v}\right]\frac{\partial T}{\partial t}\right\}, \tag{23}$$

and

$$d = \frac{\left(\frac{1}{w_v}-\frac{p}{\rho_l^* R_m T}\right)}{\left(1-\frac{p}{\rho_l^* R_m T}\right)} + \frac{p_v'}{p_v}\frac{\rho_m R_m}{\rho c_p}\left[\frac{1}{R_a}\frac{\left(h_{fg}-\frac{p}{\rho_l^*}\right)}{\left(1-\frac{p}{\rho_l^* R_m T}\right)} - T\right], \tag{24}$$

with the primed symbol above defined as $p_v' = \mathrm{d}p_v/\mathrm{d}T$. The details of the derivation of equation (20) are given by Sahota [33]. The important features of equation (20) are that it holds in the wet region so that the liquid–vapor equilibrium assumption is satisfied, and it does not contain the evaporation term Γ_m. So this equation can be solved for the pressure field in the wet region. Once the pressure is known, Γ_m is calculated from equation (19).

The initial and boundary conditions required to solve equations (19) and (20) are

$$p(x,0) = p_0(x), \tag{25}$$

$$\frac{\partial p}{\partial x}(0,t) = 0, \tag{26}$$

and

$$p(L,t) = p_\infty. \tag{27}$$

Numerical procedure

Equation (20) applies in the wet region where Γ_m is unknown. Equation (19) is the corresponding equation for the dry region with Γ_m set equal to zero. These two equations are solved simultaneously for pressure at all nodal points, and then Γ_m is calculated in the wet region from equation (19). However, new values of T and w_a are required for the solution of these equations, which can only be obtained from equations (1) and (5) if Γ_m is known. Thus equations (1), (5), (19), and (20) are solved simultaneously for T, ω_a, Γ_m, and p, after casting them in implicit finite difference form, and utilizing equations (15)–(18). New values of ρ_l and ρ_m are then calculated from equations (13) and (16). New vapor partial pressure for the dry region is obtained from equation (15). Finally, the air vapor mixture velocity is calculated from equation (9) after computing all the variable properties.

Order of magnitude analysis

The object of this section is to estimate the magnitudes of the dimensionless quantities govern-

ing heat and mass transfer in porous media. This permits selection of important terms in the governing equations and provides guidelines for the range of parameters required to describe general results.

The governing equations and boundary conditions are normalized with respect to the property datum values c_{p0}, D_0, k_0, α_0 and ρ_0, the ambient pressure p_∞, the ambient initial conditions $T_{f,0}$ and $w_{a\infty,0}$, and the length L. The definitions of the dimensionless quantities are given in the nomenclature. The resulting nondimensional governing equations and the initial and boundary conditions are given below after simplifications. These simplifications result from the order of magnitude analyses given by Sahota [33].

Energy

$$\frac{\partial\theta}{\partial\bar{t}} = \bar{\alpha}\frac{\partial^2\theta}{\partial\bar{x}^2} + \frac{1}{\bar{\rho}\bar{c}_p r}\frac{\partial}{\partial\bar{x}}(r\bar{k})\frac{\partial\theta}{\partial\bar{x}} - \frac{\bar{h}_{fg}}{\bar{\rho}\bar{c}_p}\bar{\Gamma}_m, \quad (28)$$

$$\theta(\bar{x},0) = \theta_0(\bar{x}), \quad (29)$$

$$\frac{\partial\theta}{\partial\bar{x}}(0,\bar{t}) = 0, \quad (30)$$

$$\theta(1,\bar{t}) + \frac{1}{Bi}\frac{\partial\theta}{\partial\bar{x}}(1,\bar{t}) = F(\bar{t}) - \frac{St}{Bi}\theta^4(1,\bar{t}). \quad (31)$$

Equation (28) is simply the conduction equation with a heat sink term due to evaporation of water and applies if:

(1) $\bar{\rho}_m \ll 1$ which is always the case;

(2) $C_r\bar{u}_m \ll 1$ which will mostly be the case if $\bar{u}_m$ is not too large ($\gg 10^2$) due to strong heating and if the porous medium is not too light with very low specific heat so as to make C_r larger;

(3) $C_rLe \ll 1$ which is again mostly true if the modified Lewis number is $< 10^2$ and if C_r is not too large ($\gg 10^{-3}$).

Species

$$Le\bar{D}\frac{\partial^2\bar{w}_a}{\partial\bar{x}^2} + \left[\frac{Le}{\bar{\rho}_m r}\frac{\partial}{\partial\bar{x}}(r\bar{\rho}_m\bar{D}) - \bar{u}_m\right]\frac{\partial\bar{w}_a}{\partial\bar{x}} = \frac{\bar{w}_a\bar{\Gamma}_m}{\bar{\rho}_m} \quad (32)$$

with

$$\bar{w}_a(\bar{x},0) = \bar{w}_{a,0}(\bar{x}), \quad (33)$$

$$\frac{\partial\bar{w}_a}{\partial\bar{x}}(0,\bar{t}) = 0, \quad (34)$$

and

$$\bar{w}_a(1,\bar{t}) + \frac{1}{Sh}\frac{\partial\bar{w}_a}{\partial\bar{x}}(1,\bar{t}) = \bar{w}_{a\infty}(\bar{t})$$

for a dry surface,

or
$$\bar{w}_a(1,\bar{t}) = \frac{1}{w_{a\infty,0}}\left\{\frac{1-\frac{p_v}{p}(1,\bar{t})}{1-\frac{R_v-R_a}{R_v}\left[\frac{p_v}{p}(1,\bar{t})\right]}\right\} \quad (35)$$

for a wet surface.

Equation (32) neglects $\partial\bar{w}_a/\partial\bar{t}$ and applies under moderately transient conditions when $\partial\bar{w}_a/\partial\bar{t} \ll 10^2$, since the other terms in equation (32) have an order of magnitude of 10^2.

Darcy's law

$$\bar{u}_m = -\bar{k}_D\frac{\partial\bar{p}}{\partial\bar{x}}, \quad (36)$$

with

$$\bar{p}(1,\bar{t}) = 1. \quad (37)$$

Mixture continuity

$$\frac{1}{r}\frac{\partial}{\partial\bar{x}}(r\bar{\rho}_m\bar{u}_m) = \bar{\Gamma}_m, \quad (38)$$

with

$$\bar{u}_m(0,\bar{t}) = 0. \quad (39)$$

Again the transient term $\partial\bar{\rho}_m/\partial\bar{t}$, being $\ll 0.1$ (which is the order of magnitude of the remaining terms), has been neglected in equation (38).

Liquid continuity

$$\frac{\partial\bar{\rho}_l}{\partial\bar{t}} = -\bar{\Gamma}_m, \quad (40)$$

with

$$\bar{\rho}_l(\bar{x},0) = \bar{\rho}_{l,0}(\bar{x}). \quad (41)$$

Equations of state

$$\bar{p}_v\left(\varepsilon - \frac{\rho_l}{\rho_l^*}\right) = \frac{\rho_0 R_v T_{f,0}}{p_\infty}(1 - w_{w\infty,0}\bar{w}_a)\bar{\rho}_m\theta, \quad (42)$$

and

$$\bar{p}\left(\varepsilon - \frac{\rho_l}{\rho_l^*}\right) = \frac{\rho_0 R_m T_{f,0}}{p_\infty}\bar{\rho}_m\theta. \quad (43)$$

Clausius-Clapeyron

$$\bar{p}_v = \bar{p}_{sat}(\theta). \quad (44)$$

Thus, under normal conditions of $\bar{\rho}_m \ll 1$, $C_r\bar{u}_m \ll 1$, $C_rL_e \ll 1$, and for processes which are not highly transient, i.e., $\partial\bar{w}_a/\partial\bar{t} \ll 100$ and $\partial\bar{\rho}_m/\partial\bar{t} \ll 0.1$, some reasonable simplifications can be made in the governing equations. Indeed these magnitudes suggest a simple but accurate, analysis of the temperature field may be developed by ignoring convection and diffusion.

Simple theory

If the pressure field is desired, even with the simplifications above, the solution technique discussed earlier remains the same with fewer terms in the final equations. However, if only the temperature is required, drastic simplifications can be made. In this case, equation (28) can be solved for θ with the initial and boundary conditions (29)–(31) if Γ_m is known. The following two assumptions are made to evaluate Γ_m:

1. Since under physically realistic conditions, the energy transfer due to mass diffusion is negligible compared to that by conduction, unless the mass fraction field is required for purposes other than calculating the temperature field, the species equation (32) can be dropped. Neglecting the mass diffusion term in the energy equation implies that the evaporation of water is unimportant as long as the liquid does not start to boil.

2. Since energy transfer by convection is also found to be negligible compared to conduction, Darcy's equation (36) and the gas-phase continuity (38) may also be dropped if $\bar{p}$ and $\bar{u}_m$ are not required for any other purpose. However, it should be noted that the local boiling point temperature of water depends upon the local pressure and if the local pressure is not known, the boiling point temperature is not known. Fortunately, it is observed that the saturation temperature for water is a very weak function of the saturation pressure, e.g., it only rises to 450 K at 10 atm. So the assumption is made that water always boils at 373 K. Strictly speaking, this means assuming infinite Darcy's coefficient for the purpose of calculating the temperature field.

As a result of assumption 1, $\bar{\Gamma}_m$ in equation (28) is put equal to zero at each node where temperature is less than 373 K in the wet region. $\bar{\Gamma}_m$ is likewise zero in the dry region. As the temperature at a wet node approaches 373 K, it cannot increase further according to assumption 2 unless all the liquid at that node has evaporated. Thus the temperature at all the wet nodes is kept at 373 K once this temperature is reached. So when Γ_m is nonzero, which happens only when the liquid is boiling, the temperature is known to be 373 K. Therefore equation (28) can be used to calculate the value of Γ_m. From equation (28)

$$\bar{\Gamma}_m = \frac{1}{\bar{h}_{fg}}\left[\bar{k}\frac{\partial^2\theta}{\partial\bar{x}^2} + \frac{1}{r}\frac{\partial}{\partial\bar{x}}(r\bar{k})\frac{\partial\theta}{\partial\bar{x}}\right] \qquad (45)$$

as $\partial\theta/\partial\bar{t} = 0$.

Physically, equation (45) represents a simple energy balance at a point. Usually this energy balance is used to calculate temperature, but since the temperature is known, the same energy balance gives $\bar{\Gamma}_m$. Once $\bar{\Gamma}_m$ is known, a new liquid density can be calculated at that node using equation (40). Once the liquid density becomes zero, the temperature is again allowed to increase with $\bar{\Gamma}_m = 0$.

The primary advantage of this calculation technique for the temperature is its extreme simplicity. Comparison with the complete theory shows that it gives surprisingly accurate results. The serious drawback is that it is incapable of predicting the pressures which might be of critical significance in some cases. Another drawback is that it does not take into account condensation. However, there are a wide variety of porous media where Darcy's coefficient is large and it is not necessary to calculate the pressures. This technique will be found very useful in such cases.

RESULTS AND COMPARISONS

Results

The specific case of a one-dimensional structural element with a uniform initial temperature equal to the initial temperature of the gas is considered to illustrate the results of the analysis. The element is considered to contain uniform initial moisture content from $\bar{x} = 0$–0.9 and the remaining $\bar{x} = 0.9 - 1.0$ length is supposed to be dry. The assumption of the existence of a dry region close to the surface is physically more realistic if the structure is more than a few days old. Two temperature histories are utilized to represent the extremes expected for actual fire development within structures:

(1) A long-duration, moderate-intensity fire as defined by the American Society for Testing the Materials (ASTM), E-119 standards as shown in Fig. 2 [1].

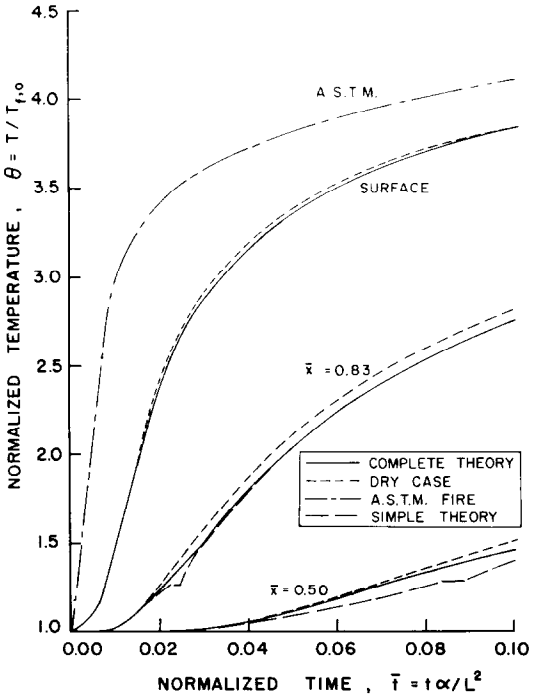

FIG. 2. Dry and wet temperature histories at different localities in the structural element for the ASTM E-119 fire time–temperature curve for $Bi = 0.5$, $\bar{k}_D = 10$, and $\bar{\rho}_{l,0} = 2.91 \times 10^{-2}$—the other parameters are listed in Table 2.

(2) A short-duration, high-intensity (SDHI) fire developed from the work of Magnusson and Thelandersson [2] as shown in Fig. 3. The standard ASTM and SDHI time-temperature curves can be extracted from Figs 2 and 3 using the thermal properties of concrete listed in Table 1 and $L = 0.15$ m.

The thermal properties of concrete are discussed by Sahota [33]. Table 1 summarizes the property values used. The corresponding dimensionless quantities are listed in Table 2. The temperature and pressure fields thus generated are given in Figs 2–7.

Figures 2 and 3 show the temperature histories given by the complete theory, the simplified analysis,

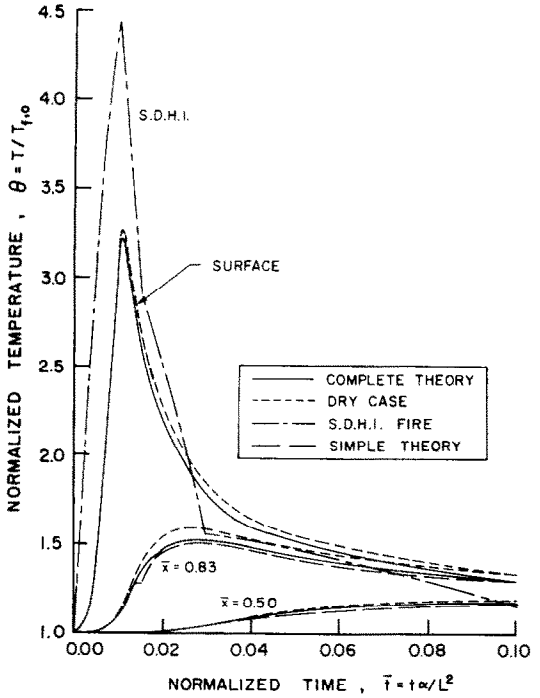

FIG. 3. Dry and wet temperature histories for the SDHI fire time–temperature curve for conditions identical to Fig. 2.

Table 1. Values of properties and dimensional parameters used in Figs 2–7

$c_p = 1140\,\mathrm{J\,kg^{-1}\,K^{-1}}$	$k_D = 6.3\times10^{-11}-\infty\,\mathrm{s\,m^3\,kg^{-1}}$
$D = 2.75\times10^{-5}\,\mathrm{m^2\,s^{-1}}$	$w_{a\infty} = 1.0$
$f = 0.9$	$\alpha = 6.39\times10^{-7}\,\mathrm{m^2\,s^{-1}}$
$h = 0-\infty$	$\varepsilon = 0.21$
$h_D = \infty$	$\rho = 2400\,\mathrm{kg\,m^{-3}}$
$k = 1.75\,\mathrm{J\,s^{-1}\,m^{-1}\,K^{-1}}$	$\rho_{l,0} = 0\text{–}210\,\mathrm{kg\,m^{-3}}$

Table 2. Values of nondimensional parameters used in Figs 2–7

$Bi = 0-\infty$	$Sh = \infty$
$\bar{c}_p = 1.0$	$St = 0.1$
$\bar{D} = 1.0$	$\bar{\alpha} = 1.0$
$\bar{k} = 1.0$	$\bar{\rho} = 1.0$
$\bar{k}_D = 10-\infty$	$\bar{\rho}_{l,0} = 0\text{–}0.1$
$L_e = 43$	

and the corresponding dry case, at the surface ($\bar{x} = 1$) and two interior points ($\bar{x} = 0.83$ and $\bar{x} = 0.50$) exposed to ASTM and SDHI fires. The value of dimensionless Darcy's coefficient, $\bar{k}_D$, used is 10. This corresponds to $k_D = 6.3\times10^{-11}\,\mathrm{s\,m^3\,kg^{-1}}$, applicable to a good quality concrete. The Biot number, Bi, is chosen to be 0.5 which corresponds to $h = 5.7\,\mathrm{J\,s^{-1}\,m^{-2}\,K^{-1}}$ for $L = 0.15\,\mathrm{m}$. The initial dimensionless liquid density, $\bar{\rho}_{l,0}$, considered is 2.92×10^{-2} which is equivalent to $\rho_{l,0} = 70\,\mathrm{kg\,m^{-3}}$, which is the amount of free water in a fully cured 1:2:4 concrete mix with an initial water/cement ratio of 0.5 by weight [33]. The temperature histories at the surface for the simple theory in Figs 2 and 3 are almost coincident with those for the complete theory and are therefore not shown.

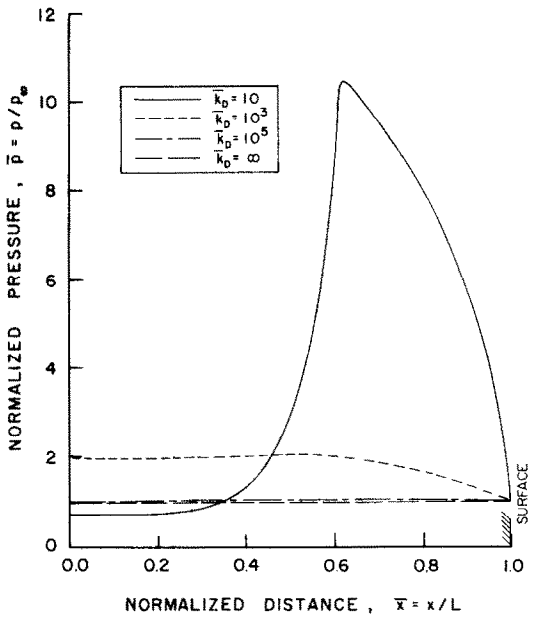

FIG. 4. Pressure profiles at $\bar{t} = 0.08$ parameterized in Darcy's coefficient for the ASTM fire time–temperature curve for conditions identical to Fig. 2.

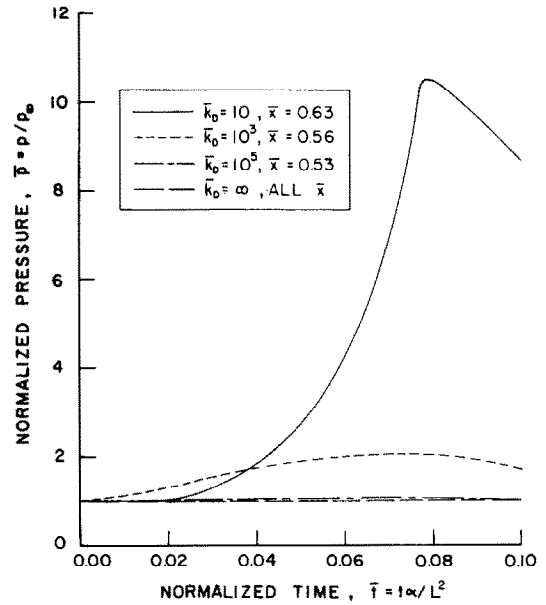

FIG. 5. Pressure histories at the maximum pressure locations parameterized in Darcy's coefficient for the ASTM fire time–temperature curve for conditions identical to Fig. 2.

It can be noted in Figs 2 and 3 that the temperatures are very close to each other for all three analyses. The temperatures for the dry and wet cases differ little due to very low amounts of moisture in concrete. For higher moisture systems the curves for the wet case are expected to shift downward making the discrepancies larger. The small differences between the simple and complete theories arise near the boiling point temperature of water at atmospheric pressure due to: (1) The

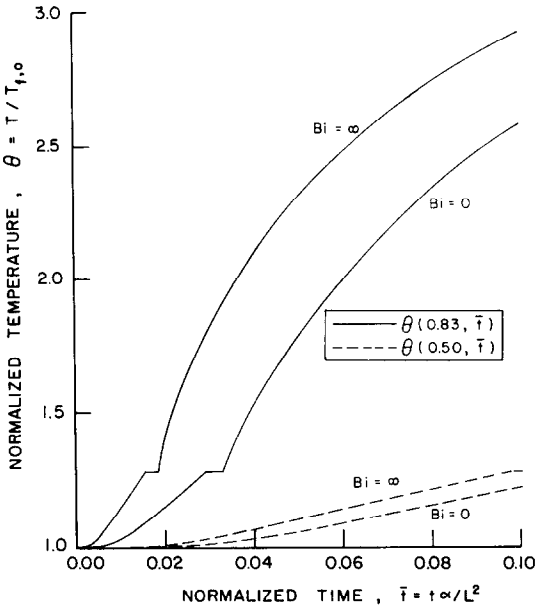

FIG. 6. Wet temperature histories, $\bar{\rho}_{l,0} = 0.1$, for simplified analysis at two locations in the structural element for the ASTM fire time–temperature curve parameterized in the Biot number, *Bi*—all other parameters are listed in Table 2.

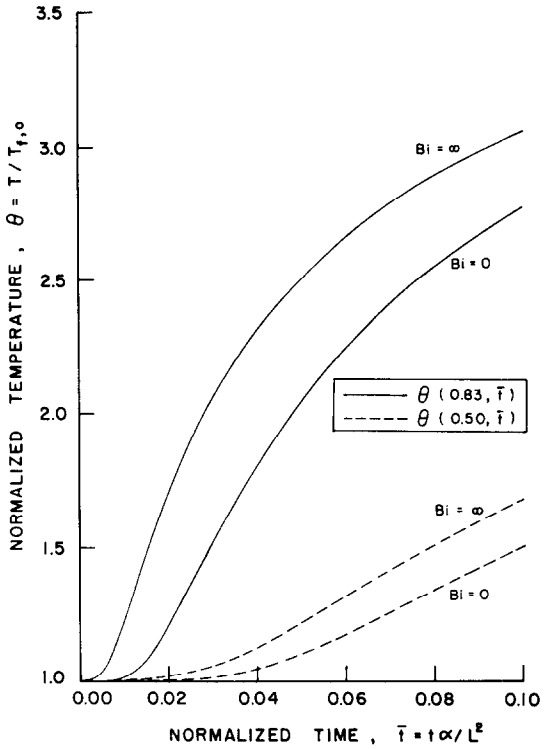

FIG. 7. Dry temperature histories, $\bar{\rho}_l = 0$, for conditions identical to Fig. 6.

pressure build up inside the element due to evaporation of water. This pressure raises the boiling point temperature of water, so that even though the temperature exceeds 373 K, it still remains below the local boiling point. The simple theory assumes an infinite Darcy's coefficient which does not allow the pressure to rise so that once the temperature reaches 373 K, no further increase is possible until all water is evaporated. However, larger discrepancies than those shown in Figs 2 and 3 are not expected as about the lowest value of k_D is used in generating these figures. Also the boiling point temperature is not sensitive to the slight changes in pressure expected in real systems. In addition, these differences are not critical to the subsequent stress analysis as they occur at low temperatures; (2) due to vapor diffusion, water must evaporate at low temperatures and act as a heat sink, keeping the temperature down. This diffusion is more dominating near the surface (this will be apparent by the decrease in the temperature plateau observed closer to the surface in Fig. 8). Since the simple theory ignores mass diffusion completely, evaporation cannot take place at temperatures lower than 373 K. Therefore the temperatures can also be overpredicted by simple theory near 373 K, as will be observed in the comparison section.

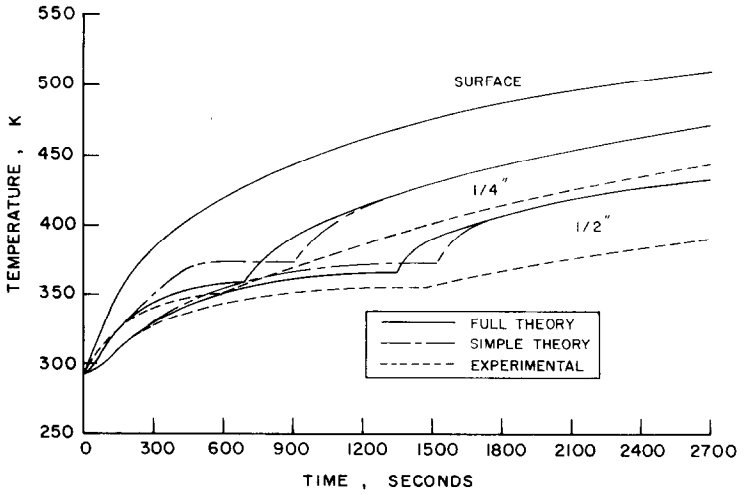

FIG. 8. Comparison of experimental and theoretical temperature histories for alumina powder—all property and parameter values are listed in Table 3.

The above two effects counteract each other. The temperatures obtained by the simple analysis are under-predicted or over-predicted near 373 K depending upon whether Darcy's coefficient is low or high, i.e. whether diffusion dominates pressure effects. These two extremes are represented by: (1) Very porous materials, such as alumina powder with a low rate of heating; and (2) good quality concrete structural members subjected to a very high rate of heating. These results and those in the comparison section show that even in the extreme cases the overall agreement between the simple and complete theories is quite good. The largest difference is near $\bar{t} = 0.08$ for $\bar{x} = 0.5$ in Fig. 2, due to the low amounts of moisture at low temperatures which are not crucial to the stress analysis. It can be concluded that as far as the temperature field is concerned, the simplified analysis can be used with very good accuracy provided $C_r\bar{u}_m \ll 1$ and $C_rLe \ll 1$, which will most often be true. Moreover, the errors generated by the inaccuracies in the thermal properties and parameters probably exceed those due to the simplified theory, (see, for example, Fig. 8).

Figures 4 and 5 show the pressure profiles and pressure histories respectively for the several values of Darcy's coefficient. The values of properties and parameters used are the same as in Figs 2 and 3. Figure 4 is drawn at a dimensionless time of 0.08, at which the maximum pressures were observed. The most probable value of $\bar{k}_D$ for a good quality concrete is 10. Therefore pressures of the order of 10 atmospheres can be expected in concrete elements exposed to fire. Such high pressures may cause spalling. Fortunately microcracking and cracking, which invariably occurs in concrete, makes it more permeable. This increases the Darcy's coefficient and therefore causes the moisture to flow more freely, thereby avoiding building up of such high pressures. Values of the order of 10^3 for $\bar{k}_D$ are found in low grade concretes or fire clay bricks. Darcy's coefficient $\approx 10^5$ corresponds to very porous materials such as sand and alumina powder. In most situations (except for small $\bar{D}$ with large $\bar{k}_D$ and $\bar{k}$ with high rate of heating) the pressure peaks are observed at the dry–wet interface which is clearly defined in the computer results. The origin side of the pressure peaks is the wet region where the air–vapor mixture flows inward and vapor condensation takes place. The surface side of the pressure peaks is the dry region. The air–vapor mixture in this region moves towards the surface. It is interesting to observe the negative pressure near the center of the element for $\bar{k}_D = 10$. This indicates specie diffusion dominating pressure induced mixture flow. Due to a low value of $\bar{k}_D$, there is much resistance to the flow of the air vapor mixture towards the center. However, due to the steep gradients in the mass fractions, the air diffuses towards outside (or the vapor diffuses inside) at high speeds relative to the mass average velocity of the air–vapor mixture. This causes the vapor to condense faster than it is replenished by the arrival of fresh mixture, thereby producing the negative pressures.

Figure 5 shows the pressure histories for these values of $\bar{k}_D$. The different locations were chosen corresponding to where the maximum pressures occurred. The maximum pressure should occur at a point reasonably far from the surface so that there is enough resistance to the flow of gases towards the surface to maintain the pressure. At the same time the point should be close enough to the surface so as to experience a reasonably high rate of heating. So there is some optimum location for peak pressures to occur corresponding to each value of Darcy's coefficient. Keeping the other parameters constant, one observes from Fig. 5 that decreasing $\bar{k}_D$ shifts the point of maximum pressure slightly towards the inside and increases its magnitude.

It can be concluded from Figs 4 and 5 that the pressure may be important in the heat and mass transfer calculations in porous media of low Darcy's coefficient, $\bar{k}_D < 10^3$, subject to increased surface temperatures. However for $\bar{k}_D > 10^3$, infinite Darcy's coefficient may safely be assumed.

Figures 6 and 7 show the temperature histories at two locations for wet and dry cases for the more commonly recognized ASTM fire. The simplified analysis was used to obtain Fig. 6 while Fig. 7, for comparison, gives the heat conduction model results. The initial dimensionless liquid density $\bar{\rho}_{l,0}$ used in Fig. 6 is 0.1. This is about the maximum amount of moisture found in concrete. Thus Figs. 6 and 7 represent the two extreme cases of initial moisture content. The Biot number, Bi, is varied from zero to infinity to obtain general limits; note that Bi does not significantly affect the temperature. Results corresponding to other Bi have thus not been plotted. The curves for $Bi \approx 10$ pass almost through the middle of $Bi = 0$ and $Bi = \infty$. For $Bi \lesssim 0.1$ the assumption of $Bi = 0$ is quite accurate. For $Bi \gtrsim 100$, the temperature boundary condition might safely be assumed. This small variation of temperatures with Bi indicates that radiation may dominate in fires since even for $Bi = 0$ the temperatures are not much different from their maximum values.

For the two extreme cases of maximum and zero liquid densities, respectively, the wet and dry results are not as close to each other as in Figs 2 and 3. The discrepancy suggests that the dry temperature may not always suffice for calculating the temperatures. In addition, had the results for the complete theory been also plotted in Fig. 6, one would have observed excellent agreement with the simple theory except for small discrepancies near 373 K. The temperature plateau in Fig. 6 for $Bi = 0$ and $\bar{x} = 0.83$ is observed to be slightly longer than for $Bi = \infty$. This indicates a slower rate of evaporation of water due to a slower local heating rate.

Comparisons

Figure 8 shows a comparison between this complete analysis, this simplified analysis, and the

experimental data of Min and Emmons [30] for alumina powder. The curves labeled 1/4 in and 1/2 in indicate the distance of the points beneath the surface. The experiments were performed on a $2\frac{1}{8}$ in long tube closed from one end and packed with alumina powder. Known quantities of water were added and the tube heated from the open end with electric lamps. The values of properties and parameters used in generating Fig. 8 are as recommended by Min and Emmons and are listed in Table 3. The temperature specified boundary condition is used.

Table 3. Values of properties and parameters used in Fig. 8

$c_p = (\rho_s c_{ps} + \rho_l c_{pl})/\rho$	$k_s = 0.75\,\mathrm{J\,s^{-1}\,m^{-1}\,K^{-1}}$
$c_{ps} = 837\,\mathrm{J\,kg^{-1}\,K^{-1}}$	$L = 0.054\,\mathrm{m}$
$c_{pl} = 4187\,\mathrm{J\,kg^{-1}\,K^{-1}}$	$w_{a\infty} = 1.0$
$C = 2.3 \times 10^{-5}\,\mathrm{m^2\,s^{-1}}$	$\varepsilon = 0.75$
$H_D = \infty$	$\rho = \rho_s + \rho_l$
$k = k_s$ in dry region	$\rho_{l,0} = 150\,\mathrm{kg\,m^{-3}}$
$= 2k_s$ in wet region	$\rho_s = 1000\,\mathrm{kg\,m^{-3}}$
$k_D = 6.42 \times 10^{-7}\,\mathrm{s\,m^3\,kg^{-1}}$	

The mixed boundary condition parameters were found unsatisfactory, since much lower surface temperature histories were obtained than reported for both dry and wet runs. Lack of agreement with the simple, analytic, dry run suggests incorrect parameters. The experimental surface temperature history, shown in Fig. 8, is not in [30] and was obtained by private communication. According to Min, the thermocouple at the surface may have overestimated the temperature due to direct radiation from the lamps and improper contact with the surface. However, the difference between the actual and the recorded surface temperatures is assumed less than the difference between the actual and the mixed boundary condition predicted surface temperature. Therefore, the measured surface temperature boundary condition was used.

Both the complete and simple theories over-predict the temperatures slightly. However, the agreement between the two theories is again excellent. As discussed earlier, this case being the high porosity extreme, the temperature by the simple theory is over-predicted when the liquid is boiling because the simple theory ignores diffusion. When all the liquid is evaporated at a given point, the simple and complete theories converge. The discrepancy between the theoretical and the experimental results is probably due to an inaccurate surface condition. It is unlikely to be due to the failure of assumptions common to both the complete and simplified analyses, such as, neglecting the movement of the liquid water and the assumption of no bound water.

CONCLUSION

An analysis is developed for one-dimensional or axi-symmetric heat and mass transfer in a wet, porous medium subject to unsteady, nonlinear, mixed, boundary conditions. The resulting equations have been solved simultaneously by an implicit finite difference technique. The numerical computations take into account condensation of the vapor in both dry and wet regions. The results clearly indicate the existence of a dry-wet interface even though no such interface has been postulated. When the pressures are not required, a simplified technique for calculating the temperature has been developed neglecting heat transfer by convection and mass diffusion. This analysis is valid for $C_r u_m \ll 1$ and $C_r Le \ll 1$. The results so obtained compared very well with the complete analysis. Comparison has been made between wet and dry cases, with the practical conclusion that for typical concrete, the dry temperature field well approximates the wet field.

An order of magnitude analysis was performed on the identified, general, governing nondimensional groups. Results have been obtained for Biot numbers varying from zero to infinity for the American Society for Testing Materials E-119 time–temperature curve. The agreement between the simplified and complete analyses, for the prediction of temperature, was found to be so good that the general results were plotted using only the simple theory. Comparison is made with experimental data on alumina powder. The agreement is acceptable.

Sumple heat conduction calculations appear to suffice for moisture contents normally found in concrete. However, if the moisture content in concrete is high ($\bar{\rho}_{l,0} \gtrsim 0.05$), as will be the case in a new structure with high initial water/cement ratio, the actual temperature may be sufficiently below that predicted by a dry heat conduction model so as to require a wet analysis. If Darcy's coefficient is low ($\bar{k}_D \lesssim 10^3$), the pressure developed inside the element might be important to the stress analysis. However, in most situations, pressures which are dangerous to the structure (>10 atmospheres) are not expected due to microcracking and cracking.

If the pressure is not required, the simplified analysis may always be used to predict the temperature field in the wet case. An exception to this will be when $C_r \bar{u}_m \gtrsim 1$ or $C_r Le \gtrsim 1$ which rarely happens in physically realistic situations. Another unimportant exception is at low temperatures, when the temperature inside the element remains below 373 K for most of the time and the evaporation takes place due to mass diffusion only. There is no difficulty in principle to extending the analysis to multi-dimensions. However, the mathematical manipulations will be much more complex. The analysis can be modified with few changes to solve a variety of other heat and mass transfer problems outlined in the Introduction. Investigation should be made regarding the importance of bound water. If the adsorption characteristics of the medium are known, it is simple to extend the present theory to do so. However, it is claimed by Sahota [33] that the maximum amount of bound water expected in concrete is less than $100\,\mathrm{kg\,m^{-3}}$. As seen in the results section, this amount is not enough to significantly affect the temperature field.

The assumption of no liquid movement was made in the development of the present theory. This assumption is probably very good for low and medium pressures. However, for very high pressures it is questionable whether the liquid does not move, particularly for high moisture content when the liquid in the different pores is interconnected. Such movement would not be difficult to incorporate. The continuity equation for the liquid will have one more term, which can be included in the subsequent calculations knowing the value of Darcy's coefficient for the liquid. A corresponding slight change would also occur in the general energy equation. More experiments on concrete are needed to provide comparisons with the present theory. These experiments should determine the temperature, pressure and moisture fields, and evaluate Darcy's coefficient for gases in concrete more accurately. Finally, some technique of calculating a pseudo thermal conductivity of wet porous media may be developed from the present work so that mass transfer effects could be included via this pseudo conductivity, $k(T)$. Simpler conduction solutions to heat transfer problems in porous media might then suffice.

Acknowledgements—This work was supported by the National Science Foundation, RANN Division and the National Bureau of Standards, Fire Research Center. We appreciate the assistance of K. Min and B. Bresler.

REFERENCES

1. Standard methods of fire tests of building construction and materials E 119-73, *Book of ASTM Standards*, p. 462. American Society for Testing and Materials, Part 14, Philadelphia (1970).
2. S. E. Magnusson and S. Thelandersson, Temperature–time curves of complete process of fire development, *Acta Polytechnica Scandanavia*, Civil Engineering and Building Construction, Stockholm, Series No. 65, Table A6, p. 136, 1970.
3. M. S. Sahota and P. J. Pagni, Temperature fields in structural elements subject to fires, *J. Heat Transfer*, **97C,** 598–604 (1975).
4. J. Becker, H. Bizri and B. Bresler, FIRES-T, A computer program for the fire response of structures—thermal, Report No. UCB FRG 74-1, Fire Research Group, University of California, Berkeley (1974).
5. J. M. Becker and B. Bresler, Reinforced concrete frames in fire environments, *J. Structural Division A.S.C.E.* **103,** 211–224 (1977).
6. H. Bizri, Structural capacity of reinforced concrete columns subjected to fire induced thermal gradients, Ph.D. dissertation, University of California, Berkeley (1973).
7. B. K. C. Chan, C. M. Ivey, and J. M. Barry, Natural convection in enclosed porous media with rectangular boundaries, *J. Heat Transfer* **92C,** 21–27 (1970).
8. Kozo Katayama and Hiroshi Nakagawa, Researches on simultaneous flow of heat and fluid through porous media, *JSME Bull.* **13,** 1013–1021 (1970).
9. Marvin E. Goldstein and Robert Siegel, Analysis of heat transfer for compressible flow in two-dimensional porous media, *Int. J. Heat Mass Transfer* **14,** 1677–1690 (1971).
10. D. S. Kim, L. E. Gates and Robert S. Brodkey, A mathematical model for heat transfer in a packed bed and a simplified solution thereof, *A.I.Ch.E. Jl* **18,** 623–627 (1972).
11. R. Seigle and M. E. Goldstein, Theory of heat transfer in a two-dimensional porous cooled medium and application to an eccentric annular region, *J. Heat Transfer* **94C,** 425–431 (1972).
12. L. A. Kozdoba and V. L. Chumakov, A system of heat and mass transfer equations for transpiration cooling, *Heat Transfer-Sov. Res.* **4,** 36–39 (1972).
13. D. M. Burch, B. A. Peavy and R. W. Allen, Time-dependent transpiration heat transfer in porous cylinders, *J. Heat Transfer* **96C,** 218–224 (1974).
14. A. V. Luikov and Y. A. Mikhailov, *Theory of Energy and Mass Transfer*. Pergamon Press, New York (1965).
15. A. V. Luikov, *Heat and Mass Transfer in Capillary porous Bodies*. Pergamon Press, New York (1966).
16. David Hansen, Walter H. Breyer and Walter J. Riback, Steady state heat transfer in partially liquid filled porous media, *J. Heat Transfer* **92C,** 520–527 (1970).
17. C. A. Chase, Dimitri Gidaspow, and R. E. Peck, Transient heat and mass transfer in an adiabatic regenerator—a Green's matrix representation, *Int. J. Heat Mass Transfer* **13,** 817–833 (1970).
18. I. J. Kumar, An extended variational formulation of the non-linear heat and mass transfer in a porous medium, *Int. J. Heat Mass Transfer* **14,** 1759–1770 (1971).
19. L. N. Gupta, An approximate solution of the generalized Stefan's problem in a porous medium, *Int. J. Heat Mass Transfer*, **17,** 313–321 (1974).
20. B. G. K. Murty, Dimitri Gidaspow and Dipak Roy, Dynamics of moisture diffusion through a partially liquid filled porous matrix, *A.I.Ch.E. Jl* **19,** 31–37 (1973).
21. L. A. Kozdoba and V. L. Chumakov, System of heat and mass transfer equations for transpiration cooling, *Heat Transfer-Sov. Res.* **5,** 117–120 (1973).
22. M. D. Mikhailov, General solutions of the diffusion equations coupled at boundary conditions, *Int. J. Heat Mass Transfer*, **16,** 2155–2164 (1973).
23. Aditya Mohan, Heat transfer in soil–water–ice systems, *A.S.C.E. J. Geotech. Div.* **101,** 97–113 (1975).
24. Donald W. Lyons, John D. Hatcher and J. Edward Sunderland, Drying of a porous medium with internal heat generation, *Int. J. Heat Mass Transfer* **15,** 897–905 (1972).
25. B. S. Krylov and V. M. Zakharov, Heat and mass transfer during evaporation of water from a porous wall, *Heat Transfer-Sov. Res.* **4,** 34–38 (1972).
26. W. A. Hull, Comparison of heat-insulating properties of materials used in fire-resistive construction, *Am. Soc. Testing Mat—Proc.* **17,** 424–452 (1917).
27. Alan Rubin and Samuel Schweitzer, Heat transfer in porous media with phase change, *Int. J. Heat Mass Transfer* **15,** 43–60 (1972).
28. Frank A. Morrison, Jr., Transient multiphase multicomponent flow in porous media, *Int. J. Heat Mass Transfer* **16,** 2331–2342 (1973).
29. T. Z. Harmathy, Simultaneous moisture and heat transfer in porous systems with particular reference to drying, *Ind. Engng Chem. Fundamentals* **8,** 92–103 (1969).
30. Kun Min and Howard W. Emmons, The drying of porous media, *Proc. 1972 Heat Transfer and Fluid Mech. Inst.*, Stanford University Press, pp. 1–18, 1972.
31. H. Saito and N. Seki, Mass transfer and pressure rise in moist porous material subjected to sudden heating, *J. Heat Transfer* **99C,** 105–112 (1977).
32. S. Schweitzer, On a possible extension of Darcy's law, *J. Hydrology* **22,** 29–34 (1974).
33. M. S. Sahota, Heat and mass transfer in porous concrete structures subject to fires, Ph.D. dissertation, Mechanical Engineering Dept., University of California, Berkeley (1976).

TRANSFERT DE CHALEUR ET DE MASSE DANS DES MILIEUX POREUX SOUMIS AU FEU

Résumé—On obtient la solution transitoire de l'écoulement biphasique et binaire dans des structures poreuses de béton, à une seule dimension ou axisymétrique, exposées à des conditions aux limites mixtes, non-linéaires et dépendant du temps. Les mécanismes considérés dans la théorie sont: conduction thermique dans tous les composants, diffusion moléculaire des composants gazeux, écoulement gouverné par la pression et obéissant à la loi de Darcy. Les équations de transfert thermique et massique sont résolues numériquement par une méthode implicite aux différences finies. Une technique simplifiée pour calculer avec l'analyse complète. Les champs de température pour les cas secs et humides ne diffèrent pas sensiblement des quantités normales d'humidité dans le béton. On donne des résultats généraux pour deux cas limites de feu: la courbe temps—température de l'American Society for Testing and Materials E-119 et une courbe de courte durée et de grande intensité. Des comparaisons entre expérience et théorie sur les champs de température sont faites pour une poudre d'alumine humide et on obtient un bon agrément. On discute les applications à des feux sur des structures et on considère une variété d'autres problèmes de transfert de chaleur et de masse.

WÄRME- UND STOFFÜBERGANG IN PORÖSEN MEDIEN- DIE FLAMMEN AUSGESETZT SIND

Zusammenfassung—Es wird die instationäre Lösung angegeben für die Zwei-Phasen-, Zwei-Komponentenströmung in eindimensionalen oder axialsymmetrischen porösen Beton-Strukturen mit zeitabhängigen, nichtlinearen, gemischten Randbedingungen. Die grundlegenden Mechanismen, die in der Theorie betrachtet werden, sind: Wärmeleitung durch alle Komponenten, die molekulare Diffusion der gasförmigen Komponenten und erzwungene Konvektion infolge einer Druckdifferenz die durch das Darcy'sche Gesetz beschrieben wird. Die maßgeblichen Wärme- und Stoffübergangsgleichungen werden mittels eines impliziten finiten Differenzenverfahrens numerisch gelöst. Zur Berechnung des Temperaturfeldes wurde eine vereinfachte Methode entwickelt; die Resultate lassen sich gut mit denen der vollständigen Lösung vergleichen. Die Temperaturfelder für den trockenen und feuchten Fall differieren nicht wesentlich bei normalem Feuchtigkeitsgehalt des Betons. Es wurden allgemeine Resultate für zwei Grenzfälle der Feuerentwicklung angegeben: die Zeit-Temperatur-Abhängigkeit E-119 der American Society for Testing and Materials und eine Kurzzeit-Hockintensitäts-Zeit-Temperatur-Abhängigkeit. Es werden experimentell und theoretisch bestimmte Temperaturfelder in einem porösen System aus feuchtem Tonerdepulver verglichen. Die Übereinstimmung ist gut. Anwendungen auf Brände in Gebäuden und eine Vielzahl anderer Wärme- und Stoffübergangsprobleme werden diskutiert.

ТЕПЛО- И МАССОПЕРЕНОС В ПОРИСТЫХ СРЕДАХ ПРИ ОБЖИГЕ

Аннотация — Получено нестационарное решение для двухфазного двухкомпонентного течения в одномерных или осесимметричных пористых бетонных структурах при наличии зависящих от времени нелинейных смешанных граничных условий. В теоретическом анализе учтены основные механизмы процесса: теплопроводность всех компонентов системы, молекулярная диффузия газовых компонентов и вызываемый разностью давлений конвективный поток, описываемый законом Дарси. Основные уравнения тепло- и массопереноса решались численно с помощью неявной конечно-разностной схемы. Разработан простой метод расчёта температурных полей и получено хорошее совпадение с результатами полного анализа. Распределения температур в сухих и влажных образцах в случае нормального содержания влаги в бетоне были в основном одинаковыми. Приведены общие результаты для двух предельных случаев обжига: кривая зависимости температуры от времени (Американское общество испытаний и материалов Е-119) и кривая зависимости температуры от времени в случае небольшой длительности и большой интенсивности процесса. Проведено сравнение между экспериментальными и теоретическими значениями распределений температур во влажном пористом алюминиевом порошке. Получено хорошее совпадение данных. Обсуждаются возможности аналогичных исследований для структурного обжига и ряда других проблем тепло- и массопереноса.